Nonlinear, three-dimensional magnetohydrodynamics of noncircular tokamaks

H. R. Strauss

Citation: The Physics of Fluids **19**, 134 (1976); doi: 10.1063/1.861310
View online: https://doi.org/10.1063/1.861310
View Table of Contents: https://aip.scitation.org/toc/pfl/19/1
Published by the American Institute of Physics

Nonlinear, three-dimensional magnetohydrodynamics of noncircular tokamaks

H. R. Strauss

Fusion Research Center, University of Texas at Austin, Austin, Texas 78712
(Received 27 May 1975)

Rosenbluth's nonlinear, approximate tokamak equations of motion are generalized to three dimensions. The equations describe magnetohydrodynamics in the low β, incompressible, large aspect ratio limit. Conservation laws are derived and a well-known form of the energy principle is recovered from the linearized equations. The equations are solved numerically to study kink modes in tokamaks with rectangular cross section. Fixed-boundary kink modes, for which the plasma completely fills the conducting chamber, are considered. These modes, which are marginally stable to lowest order in circular tokamaks, become unstable with large growth rates, comparable to the growth rates of free boundary kink modes. The unstable modes are found using linearized, two-dimensional equations. The linear results are used as initial values in the nonlinear, three-dimensional computations. The nonlinear results show that the magnetic field is perturbed only slightly, while a large amount of plasma convection takes place carrying plasma from the center of the chamber to the walls.

I. INTRODUCTION

The magnetohydrodynamic stability of plasmas to small perturbations has been the subject of a great deal of research. There has been comparatively little investigation of the nonlinear evolution of instabilities. Recently, Rosenbluth derived approximate nonlinear equations of motion for tokamaks. These equations are a great simplification of the primitive magnetohydrodynamic equations: The plasma is described by only two variables, which are functions of time and two spatial coordinates. These equations give an approximate description of kink modes in tokamaks with circular cross section. Numerical solutions by White *et al.*[1] have yielded interesting and important results, such as the formation of "bubbles" in sufficiently unstable tokamaks.

It is also of interest to investigate tokamaks with a noncircular cross section. It is conjectured that elongating the cross section will permit tokamaks to confine a higher plasma pressure for a given magnetic field strength.

In order to treat tokamaks with noncircular cross sections it is necessary to have three dimensional equations. We derive three dimensional, nonlinear, approximate tokamak equations of motion which generalize Rosenbluth's work. These equations also involve only two variables and are much simpler than the primitive equations.

From the linearized form of the equations we can obtain the approximate energy principle given by Laval *et al.*[2] The linearized equations can be Fourier analyzed in one dimension, to yield two-dimensional equations of motion. We have integrated these equations numerically, as an initial value problem, to find linearly unstable modes. We find, as suggested by results of Laval,[3] that fixed-boundary kink modes in noncircular tokamaks can have large growth rates. In circular tokamaks, such modes are stable or marginally stable in our approximation.[4] We find, however, that the stability condition is less stringent than the Kruskal–Shafranov condition $q>1$ for the cases we have considered. Thus, these modes are favorable for confinement.

The linear modes are used as starting perturbations in three-dimensional, nonlinear computations. The results show a striking contrast between small magnetic field perturbations and a substantial amount of plasma convection, which can carry plasma from the center of the chamber to the walls.

II. EQUATIONS OF MOTION

We consider a large aspect ratio tokamak. The approximation consists of ordering all quantities in the aspect ratio and dropping all toroidal effects, as well as terms of the same order as the toroidal terms. The equations then represent a long, thin plasma cylinder with periodic end conditions. (Fig. 1.)

The magnetohydrodynamic equations which we shall need are

$$\nabla \cdot \mathbf{B} = 0, \quad \nabla \times \mathbf{B} = \mathbf{j},$$

$$\frac{\partial B}{\partial t} = \nabla \times \mathbf{v} \times \mathbf{B}, \quad \rho \frac{d\mathbf{v}}{dt} = \mathbf{j} \times \mathbf{B} - \nabla p .$$

We make use of a large aspect ratio tokamak ordering. Introduce coordinates x, y, z, where z varies along the length of the plasma, and x, y are coordinates in a cross section. Scale lengths over which plasma properties vary are longer in z than in x and y by a factor of the aspect ratio. The z component of the magnetic field is larger than the x and y components by the same factor. We make the following ordering, in terms of the small quantity ϵ:

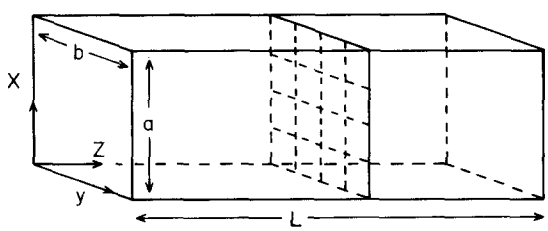

FIG. 1. Geometry and computation mesh of a rectangular tokamak.

$$\frac{\partial}{\partial x}, \frac{\partial}{\partial y} \approx 1, \quad \frac{\partial}{\partial z} \approx \epsilon, \quad B_x, B_y \approx \epsilon, \quad B_z \approx 1 + \epsilon^2,$$

$$j_x, j_y \approx \epsilon^2, \quad j_z \approx \epsilon, \quad p \approx \epsilon^2, \quad \rho \approx 1, \quad v \approx \epsilon, \quad \frac{\partial}{\partial t} \approx \epsilon.$$

Toroidal effects enter the equations of motion in order ϵ^3, although the toroidal variation of B_z due to poloidal currents in the plasma is indicated as being of order ϵ^2.

We introduce a stream function A (the z component of the vector potential) to represent the x, y, components of the magnetic field,

$$\mathbf{B} = \nabla A \times \hat{\mathbf{z}} + B_z \hat{\mathbf{z}}, \tag{1}$$

where $\hat{\mathbf{z}}$ is the unit vector in the z direction. The divergence of $\mathbf{B}$ is then

$$\nabla \cdot \mathbf{B} = \partial B_z / \partial z \approx \epsilon^3 .$$

We neglect ϵ^3 terms so that within our approximation $\mathbf{B}$ is divergence-free.

Examination of the momentum equation shows that we can neglect the z component of the force, so that v_z can be set to zero,

$$v_z = 0 . \tag{2}$$

The flux equation can be integrated by introducing the vector potential for $\mathbf{B}$:

$$\frac{\partial}{\partial t}\mathbf{A} = \mathbf{v} \times \mathbf{B} + \nabla \phi ,$$

where ϕ is a gauge potential. The x and y components of this equation, which give the variation of B_z, must be ϵ^3 according to our ordering; the variable part of B_z is of order ϵ^2. We obtain

$$\frac{\partial}{\partial t}\mathbf{A} \times \hat{\mathbf{z}} = -B_z \mathbf{v} + \nabla \phi \times \hat{\mathbf{z}} = 0 .$$

This shows we can introduce a stream function U for $\mathbf{v}(\phi = B_z U)$:

$$\mathbf{v} = \nabla U \times \hat{\mathbf{z}}, \quad \nabla \cdot \mathbf{v} = 0 . \tag{3}$$

Because of the large, constant, longitudinal magnetic field, the flow is incompressible. Using this result in the z component of the flux equation, we find

$$\frac{\partial A}{\partial t} = \nabla U \times \nabla A \cdot \hat{\mathbf{z}} + B_z \frac{\partial U}{\partial z}, \tag{4}$$

which can be expressed as

$$\frac{\partial A}{\partial t} = \mathbf{B} \cdot \nabla U$$

or as

$$\frac{\partial A}{\partial t} + \mathbf{v} \cdot \nabla A = B_z \frac{\partial U}{\partial z} .$$

Taking the curl of $\mathbf{B}$ yields the current

$$j_z = -\nabla_\perp^2 A, \quad \mathbf{j}_\perp = \nabla B_z \times \hat{\mathbf{z}} + \nabla_\perp \frac{\partial A}{\partial z}, \tag{5}$$

where

$$\nabla_\perp = \nabla - \hat{\mathbf{z}} \frac{\partial}{\partial z}, \tag{6}$$

$$\nabla_\perp^2 = \frac{\partial^2}{\partial x^2} + \frac{\partial^2}{\partial y^2} . \tag{7}$$

The z derivatives in the Laplacian are of higher order and can be dropped. This is a great advantage in solving the equations numerically.

Substituting $\mathbf{j}$ into the momentum equation we find that

$$\rho \frac{d\mathbf{v}}{dt} = B_z \frac{\partial}{\partial z} \nabla_\perp A \times \hat{\mathbf{z}} - \nabla_\perp^2 A \nabla_\perp A - \nabla_\perp (p + \tfrac{1}{2} B_z^2) . \tag{8}$$

For simplicity, we consider constant density, setting

$$\rho = 1.$$

We can now eliminate both the pressure and the spatially varying part of B_z by taking the curl. The result can be written, along with the flux equations, as

$$\frac{\partial \nabla_\perp^2 U}{\partial t} = -\mathbf{v} \cdot \nabla \nabla_\perp^2 U + \mathbf{B} \cdot \nabla \nabla_\perp^2 A , \tag{9}$$

$$\frac{\partial A}{\partial t} = \mathbf{B} \cdot \nabla U . \tag{10}$$

These are our nonlinear, three-dimensional approximate tokamak equations of motion, giving the rate of change of vorticity and magnetic flux.

In the following we shall consider plasmas bounded by a conducting wall. The boundary conditions are

$$\hat{\mathbf{n}} \cdot \mathbf{B} = \hat{\mathbf{n}} \cdot \mathbf{v} = 0 ,$$

where $\hat{\mathbf{n}}$ is normal to the wall, or

$$A = U = 0 \tag{11}$$

at the wall. For the case of plasma surrounded by a vacuum, the boundary conditions are more complex and will be given elsewhere.

III. CONSERVATION LAWS

The equations we have derived conserve energy and magnetic flux. The linearized equations yield the energy theorem of Laval *et al.*[2]

The nonlinear energy theorem takes a particularly simple form. Multiplying the vorticity equation (9) by U,

$$\begin{aligned} U \frac{\partial \nabla_\perp^2 U}{\partial t} &= -U\mathbf{v} \cdot \nabla \nabla_\perp^2 U + U\mathbf{B} \cdot \nabla \nabla_\perp^2 A \\ &= \nabla \cdot (-U \nabla_\perp^2 U \mathbf{v} + U \nabla_\perp^2 A \mathbf{B}) - \nabla_\perp^2 A (\mathbf{B} \cdot \nabla U) \\ &= -\frac{\partial A}{\partial t} \nabla_\perp^2 A . \end{aligned}$$

In the last line, we have set the divergence term equal to zero, because it makes no contribution when we integrate over the plasma volume and apply the boundary condition $U = 0$. We have also made use of the flux equation (10). Integrating this equation, we have the energy theorem

$$\frac{\partial}{\partial t} \int dx\, dy dz [(\nabla_\perp U)^2 + (\nabla_\perp A)^2] = 0 . \tag{12}$$

The two terms clearly represent kinetic and potential energy. Because the flow is incompressible, the pressure and $(B_z)^2$ do not contribute to the energy.

The conservation of flux implies the existence of magnetic surfaces. Given a function S moving with the fluid, which satisfies

$$\frac{\partial S}{\partial t} + \mathbf{v} \cdot \nabla S = 0 , \tag{13}$$

then we can show from the flux equation (10) that

$$\frac{\partial}{\partial t}(\mathbf{B} \cdot \nabla S) + \mathbf{v} \cdot \nabla(\mathbf{B} \cdot \nabla S) = 0 . \tag{14}$$

If S represents magnetic surfaces satisfying

$$\mathbf{B} \cdot \nabla S = 0 \tag{15}$$

initially, then this relation will continue to hold as the plasma moves about. Note that if A is independent of z, as we shall assume in finding equilibrium states, then S is a function of A.

Let us now consider the linearized equations. The equilibrium conditions are, from (9) and (10),

$$\frac{\partial A}{\partial t} = U = 0 .$$

If the equilibrium is independent of z, we have

$$\frac{\partial A}{\partial z} = 0 , \qquad \nabla_\perp^2 A = -j(A) .$$

Expanding about an equilibrium specified by A_0, we add small perturbations A_1 and U_1:

$$A = A_0 + A_1 , \qquad U = U_1 .$$

The equations of motion become

$$\frac{\partial A_1}{\partial t} = \mathbf{B}_0 \cdot \nabla U_1 , \tag{16}$$

$$\frac{\partial \nabla_\perp^2 U_1}{\partial t} = \mathbf{B}_0 \cdot \nabla \nabla_\perp^2 A + \nabla j_0 \times \nabla A_1 \cdot \hat{\mathbf{z}} . \tag{17}$$

Differentiating the vorticity equation with respect to time and substituting for $\partial A_1/\partial t$ from the flux equation gives

$$\frac{\partial^2}{\partial t^2} \nabla_\perp^2 U_1 = \mathbf{B} \cdot \nabla \nabla_\perp^2 (\mathbf{B}_0 \cdot \nabla U_1) + \nabla j_0 \times \nabla (\mathbf{B}_0 \cdot \nabla U_1) \cdot \hat{\mathbf{z}} . \tag{18}$$

From this we can easily derive an energy principle. Multiplying by U_1, assuming a time dependence $\exp(\gamma t)$, integrating over the plasma volume, and integrating by parts yields the energy principle

$$-\gamma^2 \int dV (\nabla_\perp U)^2 = \int dV [(\nabla_\perp (\mathbf{B}_0 \cdot \nabla U))^2 + (\mathbf{B}_0 \cdot \nabla U) \nabla j_0 \times \nabla U \cdot \hat{\mathbf{z}}] . \tag{19}$$

Finally, we show how the nonlinear equations are simplified if we assume helical symmetry. This means that if we introduce polar coordinates r, θ for x, y so that

$$\frac{\partial}{\partial z} = \frac{k}{m} \frac{\partial}{\partial \theta} ,$$

the flux equation then becomes

$$\frac{\partial A}{\partial t} + \mathbf{v} \cdot \nabla A = \frac{B_z k}{m} \frac{\partial U}{\partial \theta} = \frac{B_z k}{2m} \mathbf{v} \cdot \nabla r^2 .$$

Therefore the flux ψ is conserved,

$$\psi = A - B_z k r^2 / 2m , \tag{20}$$

$$\frac{\partial \psi}{\partial t} + \mathbf{v} \cdot \nabla \psi = 0 . \tag{21}$$

Also, the gradient along $\mathbf{B}$ of a helically symmetric function f becomes

$$\mathbf{B} \cdot \nabla f = \nabla f \times \nabla \psi \cdot \hat{\mathbf{z}}$$

and the vorticity equation is simplified to

$$\frac{\partial \nabla_\perp^2 U}{\partial t} = -\mathbf{v} \cdot \nabla (\nabla_\perp^2 U) + \nabla \nabla_\perp^2 \psi \times \nabla \psi \cdot \hat{\mathbf{z}} . \tag{22}$$

These are the helically symmetric equations given by Rosenbluth.

Having derived the tokamak equations of motion and discussed some of their consequences, we now investigate some solutions.

IV. EQUILIBRIUM

We apply the equations to the study of tokamaks with noncircular cross sections. For simplicity, we restrict the problem to rectangular cross sections. In that case the numerical method can be based on a simple rectangular mesh.

In this paper we examine the stability of a special class of equilibrium solutions, as in Bateman *et al.*[5] and Wooten *et al.*,[6] although their results do not apply to the incompressible limit described by our equations.

The equilibrium is given by

$$A = A_0 \cos\frac{\pi x}{a} \cos\frac{\pi y}{b} , \quad -\frac{a}{2} \le x \le \frac{a}{2} , \quad -\frac{b}{2} \le y \le \frac{b}{2} . \tag{23}$$

The current is proportional to A, and like A, vanishes at the walls. The constant A_0 determines the current flowing in the plasma and hence, the stability of the plasma. The walls enclosing the plasma have width a, height b, and length L.

The basic measure of magnetohydrodynamic stability is the rotational transform, or its inverse q, which is defined as

$$q = \frac{B_z}{L} \oint \frac{ds}{|\nabla A|} = \frac{B_z}{L} \frac{dV}{dA} .$$

Here, V is the area contained within a contour of constant A. For the equilibrium A, we have

$$V = \int y\, dx = \frac{ab}{\pi^2} \int \cos^{-1}\left(\frac{A}{(A_0 \cos(\pi x/a)}\right) dx ,$$

where we have substituted for y from the equation for $A(x, y)$. Differentiating V with respect to A gives a result which can be transformed into an elliptic integral. We find

$$q = \frac{4ab B_z}{\pi^2 A_0 L} K(\sin\phi) , \qquad \cos\phi = \frac{A}{A_0} , \tag{24}$$

where K is an elliptic integral of the first kind. The graph of q as a function of x shows that q is fairly constant over a large area of the plasma, while becoming

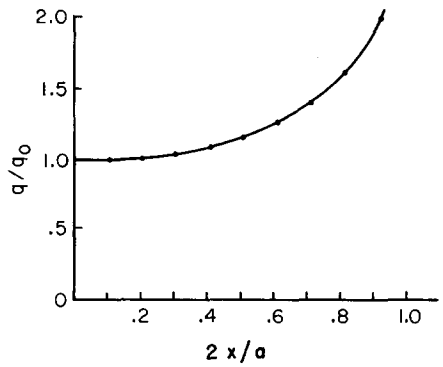

FIG. 2. Inverse rotational transform q as a function of distance from the magnetic axis, $2x/a$.

infinite at the boundary. This is due to the sharp corners in the boundary which force magnetic field lines to become straight. The effect is quite localized near the edge of the plasma (Fig. 2).

Values of q less than unity are associated with instability. The plasma is more unstable in the center, where the values of q are lower.

V. NUMERICAL METHODS

The same numerical methods[7] were applied to the two-dimensional linear equations and the three-dimensional nonlinear equations.

We used a simple Eulerian treatment of the equations, based on a rectangular mesh. The spatial derivatives were put into standard, second-order accurate finite difference form. For example,

$$\frac{\partial A}{\partial x} = [A(I+1) - A(I-1)]/2DX .$$

The variables A and U are functions of the mesh points (I, J, K). To advance the solution in time, the leapfrog method was used. This replaces a first-order time derivative by a second-order accurate finite time difference:

$$\frac{\partial f}{\partial t} = g$$

becomes

$$f^{N+1}(I,J,K) = f^{N-1}(I,J,K) = 2DTg^{N}(I,J,K)$$

where the superscripts refer to time levels.

The equations are complicated by the presence of the Laplace operator. In order to find U and thus the velocity, it is necessary to solve Poisson's equation at every time step. This is accomplished efficiently by a direct method using fast Fourier transforms. About half of the computation time was spent solving Poisson's equation. Fortunately, the Poisson equation is only two-dimensional!

The numerical stability can be estimated by considering the linearized equation with B constant,

$$\frac{\partial A}{\partial t} = B\cdot\nabla U, \quad \frac{\partial U}{\partial t} = B\cdot\nabla A .$$

The difference form of these equations can then be Fourier analyzed. For a mode varying as $\exp(ikx)$ and with

$$A^{N+1} = \lambda A^{N},$$

we find a Courant condition for numerical stability in form

$$B_x(DT/DX) + B_y(DT/DY) + B_z(DT/DZ) < 1 . \qquad (25)$$

Since the perturbation of B tended to be small, there was no need to vary DT.

To avoid storing the vorticity as well as U, we integrated the vorticity equation,

$$\frac{\partial U}{\partial t} = F + B_z\frac{\partial A}{\partial z} + \mu\nabla_1^2 U, \quad \nabla_1^2 F = [\nabla_1^2 A, A] - [\nabla_1^2 U, U], \qquad (26)$$

where

$$[A, B] = \frac{\partial A}{\partial x}\frac{\partial B}{\partial y} - \frac{\partial A}{\partial y}\frac{\partial B}{\partial x} .$$

We added a viscosity μ to damp the highest Fourier harmonics. This term was handled using the Dufort–Frankel technique. A similar resistivity was added to Eq. (10). However, these damping terms were not required for numerical stability.

We also solved the magnetic surface equation (13) in order to study the flow. Because S developed large gradients, it was found desirable to introduce some smoothing to suppress the highest harmonics. This was also done in calculating the current from Eq. (5).

In the nonlinear calculations, it was found that the solutions had half-wavelength symmetry. The solution at $z = L/2$ was equal to the solution at $z = 0$, but rotated 180°. Taking advantage of this symmetry reduced the storage requirements by half.

VI. LINEAR STABILITY

We now apply our equations to study the linear stability of the equilibria described in Sec. III. Starting with an arbitrary initial perturbation we integrate the linear equations forward in time. If the equilibrium is unstable, the unstable modes will grow exponentially and the mode with the largest growth rate will dominate the solution after a sufficiently long time.

The linear equations (16) and (17) can be Fourier analyzed in z, since the equilibrium is independent of z. The linear perturbations have the form

$$A_1 = A_s\sin kz + A_c\cos kz, \quad U_1 = U_s\sin kz + U_c\cos kz . \qquad (27)$$

Both components are required. This gives four coupled linear equations for A_s, A_c, U_s, and U_c.

The results show that the internal kink mode can be unstable, with large growth rates comparable to the free boundary kink modes. The growth rates are given in units of $(B_z/L)^{-1}$, the inverse of the longitudinal Alfvén transit time, and are of order unity. In Figs. 3 and 4 we show results for the case $b/a = 2$. The unstable modes shown have what may be called an $m = 1$, $n = 1$ structure, as can be seen from Figs. 4 and 5.

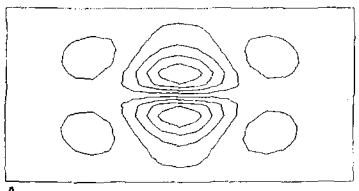

FIG. 3. A linearly unstable mode at $z=0$, with $b/a=2$, $q_0=0.838$, and growth rate 0.423.

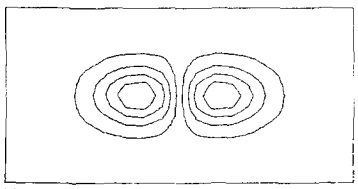

The growth rate increases as we increase the plasma current. We measure the current in terms of q_0, the inverse rotational transform in the center of the plasma, given by Eq. (24). As q_0 decreases, the unstable mode fills more of the plasma, as shown in Fig. 5. In Fig. 6 we plot the growth rate as a function of q_0. The two curves show the influence of the finite difference grid. Increasing the number of mesh points shifts the marginal stability point to larger q_0, presumably because the more localized structure is better resolved. The onset of instability occurs for $q_0<1$, so these modes are favorable for confinement.

It is of interest to consider the equation describing plasma flow (12). Linearizing, and taking S_0 equal to A_0, we find

$$\frac{\partial S_1}{\partial t} = -v_1 \cdot \nabla S_0 = B_1^0 \cdot \nabla U_1 = \frac{\partial A_1}{\partial t} - B_z \frac{\partial U_1}{\partial z} .$$

For a mode with growth rate γ, Fourier analysis in z yields

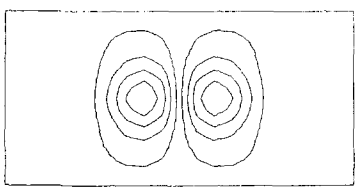

FIG. 4. The same mode at $z=L/4$.

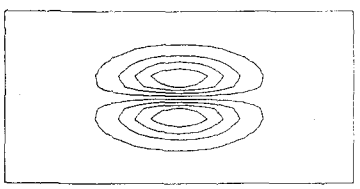

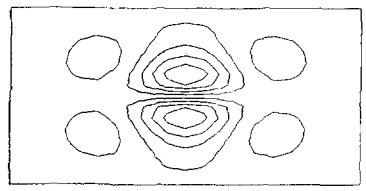

FIG. 5. Effect of increasing equilibrium current: the growth rate increases and the mode structure spreads out.

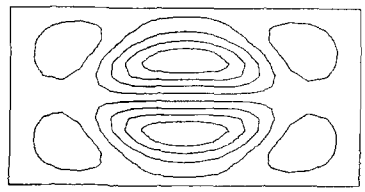

$$S_s = A_s + (2\pi/\gamma) U_c ,$$

where γ is in units of $(B_z/L)^{-1}$. Typically, $U_c \gtrsim A_s$; so for small growth rate, $\delta S/S \gg \delta A/A$. This effect is quite evident in the nonlinear results.

VII. NONLINEAR MOTION

The linearly unstable modes can be used as initial perturbations in three-dimensional nonlinear computations using Eqs. (9) and (10). The quantities A and U by themselves do not show the plasma motion, so we have also integrated the auxiliary equation (13), which describes the convection of a quantity S with the fluid. In the unperturbed initial state, S is proportional to A^2. In addition, we examined the longitudinal current density j, as calculated from Eq. (5).

Some sample results are shown in Figs. 7–12. Contour plots of A, S, U, and j are given for $z=0$ and $z=L/4$. The solutions for $z=L/4$ are basically the same as the solutions at $z=0$, but rotated 90°.

There is a striking difference in the time develop-

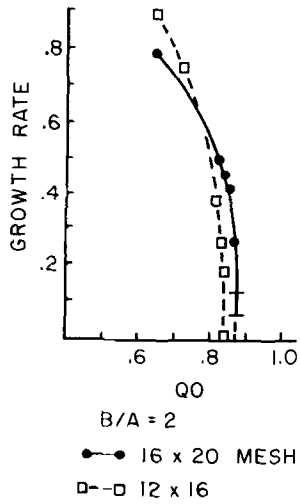

FIG. 6. Growth rate in units of the longitudinal Alfvén time, $\rho^{1/2}L/B_z$.

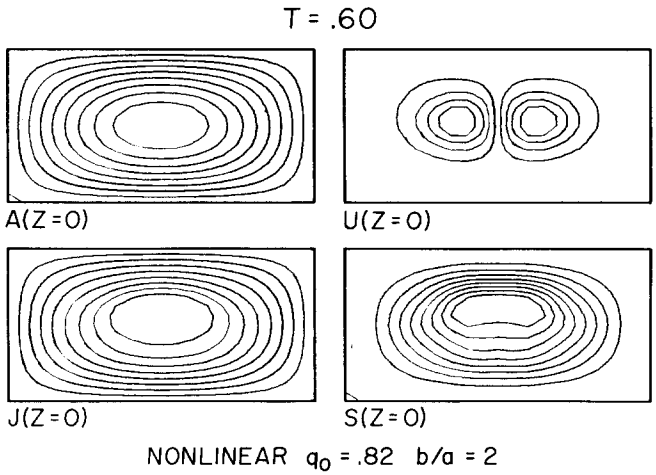

FIG. 7. A nonlinear calculation. The plane $z=0$ is shown at time $T=0.6$ in units $\rho^{1/2}L/B_z$. The four plots show the magnetic vector potential A, the longitudinal current density J, the flow streamlines U, and magnetic surfaces S. The q value on axis of the starting equilibrium is 0.82; the width of the cross section is twice the height.

ment of A and S. The perturbations of A, and consequently the perturbations of the magnetic field, are limited in amplitude and confined to the center of the plasma. On the other hand, the contours of S are strongly perturbed, showing convection of the plasma from the center of the chamber to the walls. The contours of U are the streamlines of the flow, according to Eq. (3). The linear flow pattern of Figs. 4 and 5 is maintained in the early stage of the nonlinear calculation, causing plasma to flow outward toward the wall (Figs. 7 and 8). Then, the flow pattern U is itself convected outward, as in Figs. 9 and 10. This produces a pinching of the flux surfaces S in the center, as well as a continued outward flow to the wall (Figs. 11 and 12). Calculation of the energy, Eq. (12), showed that the kinetic energy in the calculation just discussed was less than 2% of the magnetic potential energy.

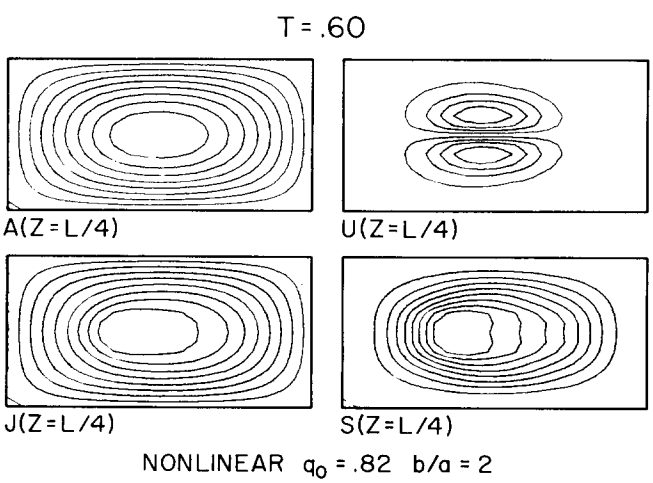

FIG. 8. The plane $z=L/4$ at the same time as Fig. 7. The perturbations are rotated at quarter turn.

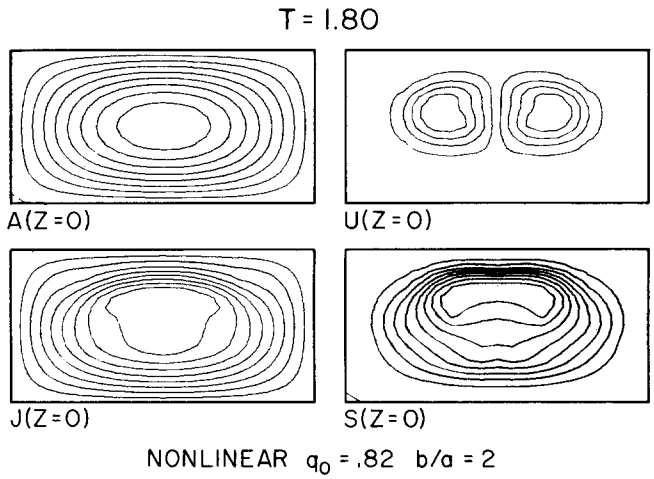

FIG. 9. The same as Fig. 7 but at time $T=1.8$. Convection is shown by the contours of S.

It is remarkable that the contours of A are disturbed so little, while the contours of S and j are strongly perturbed. The difference between A and j can be understood by Fourier analyzing Eq. (5) in x and y. For the m, n component we have

$$j_{mn} = -\pi^2[(m/a)^2 + (n/b)^2]A_{mn} .$$

The factor in brackets strongly attenuates the short wavelength perturbations of j, so that A seems almost unchanged.

It is also possible that numerical diffusion has allowed the plasma to slip through the magnetic field to some extent. This effect can only be assessed by the use of more refined numerical methods in which the magnetic field lines are rigorously constrained to lie on magnetic surfaces, i.e., $\mathbf{B}\cdot\nabla S=0$ exactly.

VIII. CONCLUSIONS

We have presented a set of equations describing magnetohydrodynamic motion in a large aspect ratio tokamak. The equations are much simpler than the full set

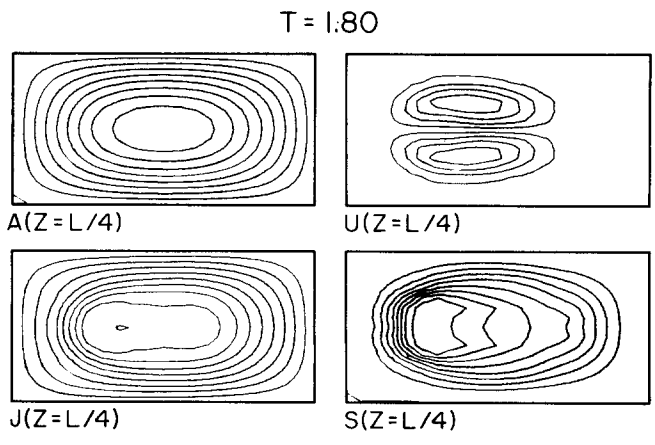

FIG. 10. The plane $z=L/4$ at $T=1.8$; similar to Fig. 9.

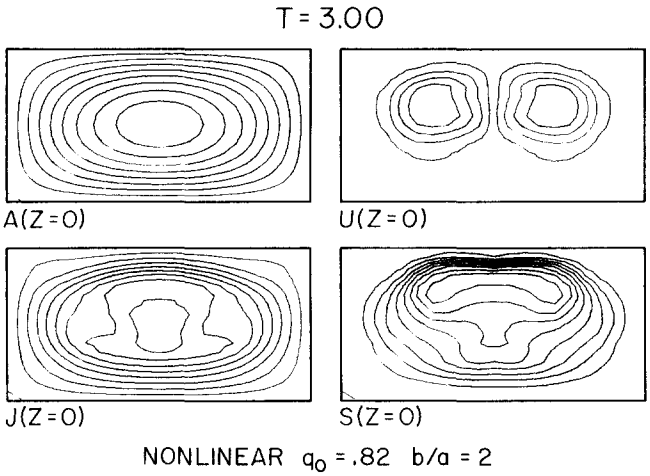

FIG. 11. The same as Fig. 7 at time $T=3.0$. Substantial convection has taken place, as shown by S. The poloidal magnetic field is tangent to the contours of A, which are hardly perturbed. The current J shows greater perturbation. The flow pattern of U itself convects toward the wall.

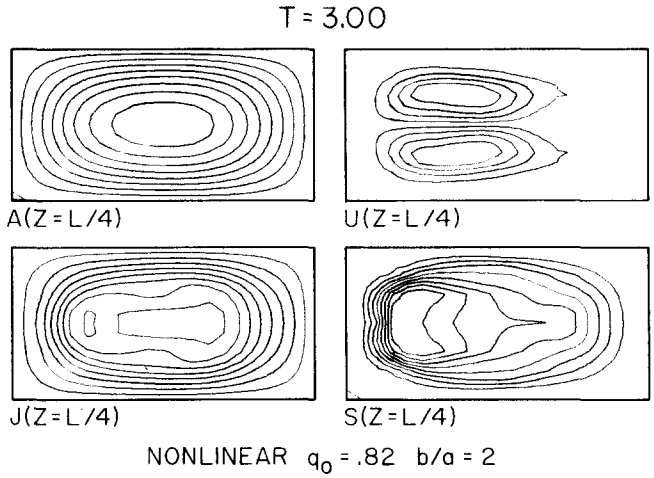

FIG. 12. The plane $z=L/4$ at $T=3.0$, similar to Fig. 11.

of magnetohydrodynamic equations. Numerical solution of the equations has confirmed the existence of fast-growing fixed-boundary kink modes in noncircular tokamaks. The onset condition for instability, in the cases we have investigated, is less stringent than the Kruskal–Shafranov condition $q>1$. The nonlinear development of these instabilities was also investigated numerically. The results show that small magnetic field perturbations are accompanied by substantial plasma convection.

ACKNOWLEDGMENTS

The author expresses his appreciation to Marshall Rosenbluth for his interest in this work. Thanks also to those who gave valuable computing advice: George Bourianoff, Adam Drobot, Alan Macmahon, and Michael Sternberg. This work was supported by the U. S. Energy Research and Development Administration Contract No. AT-(40-1)-4478.

[1]R. White, D. Monticello, M. N. Rosenbluth, H. Strauss, and B. B. Kadomtsev, in *Plasma Physics and Controlled Nuclear Fusion Research*, Tokyo, (International Atomic Energy A Agency, Vienna, 1975), paper CN-33/A 13-3.
[2]G. Laval, R. Pellat, and J. Soule, Phys. Fluids **17**, 4 (1974).
[3]G. Laval, Phys. Rev. Lett. **34**, 1316 (1975).
[4]V. D. Shafranov, Zh. Tekh. Fiz. **40**, 241 (1970) [Sov. Phys. Tech. Phys. **15**, 175 (1970)].
[5]G. Bateman, W. Schneider, and W. Grossmann, Nucl. Fusion **14**, 5 (1974).
[6]J. Wooten, H. R. Hicks, G. Batemann, and R. A. Dory (to be published).
[7]All numerical methods are described in P. J. Roache, *Computational Fluid Dynamics* (Hermosa, Albuquerque, New Mexico, 1972) and in R. Richtmyer and K. Morton, *Difference Methods for Initial-Value Problems* (Wiley, New York, 1967).